Takemura *et al. Earth, Planets and Space* (2016) 68:166
DOI 10.1186/s40623-016-0544-8

Earth, Planets and Space

LETTER

Open Access

Prediction of maximum *P*- and *S*-wave amplitude distributions incorporating frequency- and distance-dependent characteristics of the observed apparent radiation patterns

Shunsuke Takemura[1*], Manabu Kobayashi[2] and Kazuo Yoshimoto[2]

Abstract

Frequency-dependent model of the apparent radiation pattern has been extensively incorporated into engineering and scientific applications for high-frequency seismic waves, but distance-dependent properties have not yet been fully taken into account. We investigated the unified characteristics of frequency and distance dependences in both apparent *P*- and *S*-wave radiation patterns during local crustal earthquakes. Observed distortions of the apparent *P*- and *S*-wave radiation patterns could be simply modeled by using a function of the normalized hypocentral distance, which is a product of the wave number and hypocentral distance. This behavior suggests that major cause of distortion of the apparent radiation pattern is seismic wave scattering and diffraction within the heterogeneous crust. On the basis of observed normalized hypocentral distance dependency, we proposed a method for prediction of spatial distributions of maximum *P*- and *S*-wave amplitudes. Our method incorporating normalized hypocentral distance dependence of the apparent radiation pattern reproduced the observed spatial distributions of maximum *P*- and *S*-wave amplitudes over a wide frequency and distance ranges successfully.

Keywords: Body waves, Wave propagation, Earthquake ground motions

Introduction

It is well known that, as frequency increases over 1 Hz, the spatial distributions of observed maximum *P*- and *S*-wave amplitudes during local earthquakes (hereafter, this is called the "apparent radiation pattern") are gradually distorted from the expected four-lobe amplitude pattern of a double-couple point source (e.g., Liu and Helmberger 1985; Satoh 2002a; Takenaka et al. 2003; Takemura et al. 2009; Sawazaki et al. 2011; Kobayashi et al. 2015). The frequency-dependent characteristics of the observed apparent radiation patterns have been incorporated into various applications such as the predictions of strong ground motions (e.g., Pitarka et al. 2000; Pulido and Kubo 2004), the estimation of high-frequency seismic energy radiation during large earthquakes (e.g., Nakahara 2013), nonvolcanic/volcanic tremors (e.g., Maeda and Obara 2009; Kumagai et al. 2010; Cannata et al. 2013; Yabe and Ide 2014), and landslides (e.g., Ogiso and Yomogida 2015), and the earthquake early warning systems (e.g., Okamoto and Tsuno 2015). Although the frequency–distance change model for *S*-wave radiation pattern proposed by Satoh (2002b) has been used in some applications, to achieve more accurate estimation and prediction of high-frequency seismic radiation, a precise frequency- and distance-dependent model for the apparent radiation pattern for both *P* and *S* waves is required. Relationship of the apparent radiation patterns between *P* and *S* waves has been important due to recent development real-time systems, such as urgent

*Correspondence: shunsuke@bosai.go.jp
[1] National Research Institute for Earth Science and Disaster Resilience, 3-1 Tennodai, Tsukuba 305-0006, Japan
Full list of author information is available at the end of the article

earthquake detection and earthquake early warning (e.g., Okamoto and Tsuno 2015).

High-quality seismograms recorded by dense regional seismic networks for various distances and wide dynamic ranges enable us to investigate frequency- and distance-dependent characteristics of the apparent radiation pattern. Takemura et al. (2009, 2015) and Kobayashi et al. (2015) reported that the apparent *P*- and *S*-wave radiation patterns are distorted with increasing distance but still preserving the original four-lobe pattern at hypocentral distances less than 40 km even for high frequencies. In this study, we firstly investigated the frequency- and distance-dependent characteristics of the apparent *P*- and *S*-wave radiation patterns using dense and large number seismograms. On the basis of observed characteristics, then we propose a frequency- and distance-dependent model of the apparent radiation pattern to predict the spatial distributions of maximum *P*- and *S*-wave amplitudes of local earthquakes.

Apparent radiation pattern for crustal earthquakes

We analyzed velocity waveforms recorded by Hi-net (high-sensitivity seismograph network operated by the National Research Institute for Earth Science and Disaster Resilience (NIED); Okada et al. 2004) during 13 earthquakes occurred in the crust of Chugoku region, Japan (Events 1–13 of Fig. 1a and Additional file 1: Table S1). The mechanisms of these earthquakes were characterized by strike-slip faulting and reported consistently by both the moment tensor (MT) solutions of F-net (full range seismograph network by NIED; Fukuyama et al. 1998) and the first-motion focal mechanisms in the unified hypocenter catalog of the Japan Meteorological Agency.

In some previous studies, energy partition of *S* wave in each horizontal component was analyzed in order to eliminate the effects of differences in site amplification and source size. However, Sawazaki et al. (2011) pointed out that spatial distribution of maximum amplitudes and energy partitioning in each component show different frequency-dependent properties. Therefore, on the basis of the method by Kobayashi et al. (2015), we measured coda-normalized maximum *P*- and *S*-wave amplitudes (hereafter, these are referred to as the "*P*-wave amplitude" and "*S*-wave amplitude," respectively) from three-component root-mean-square (RMS) envelopes for the following different frequency bands: 0.5–1, 1–2, 2–4, 4–8, and 8–16 Hz.

Additional file 1: Figure S1 shows examples of filtered velocity seismograms and RMS vector envelopes normalized by averaged coda amplitudes to eliminate the effects of differences in site amplification and source size (e.g., Yoshimoto et al. 1993). Since coda normalization technique is applicable in the seismograms with hypocentral distance less than approximately 150 km (e.g., Sato et al. 2012 Ch. 3; Takemoto et al. 2012), we employ the lapse times of 60–70 s for calculating averaged coda amplitudes. The time windows of τ-seconds, which represent the averaged pulse durations of *P* and *S* waves measured from the displacement waveforms at four F-net stations (filled triangles in Fig. 1a), were used to measure *P*- and *S*-wave amplitudes.

After measuring *P*- and *S*-wave amplitudes, we estimated the master attenuation curves of *P*- and *S*-wave attenuations by using the following equation:

$$\ln\left(L_i A_{ij}^{\max}\right) = -\frac{\pi f_C}{Q_j V_j} L_i + B \quad (j = P, S), \tag{1}$$

where $A_{ij}^{\max}$ is the *P*- or *S*-wave amplitude at a hypocentral distance of L_i km, Q_j is the quality factor for the apparent *P*- or *S*-wave attenuation, f_C is the central frequency of each band, V_j is the seismic velocity for *P* or *S* waves in the upper crust (assuming 6.00 and 3.55 km/s, respectively), and *B* is a constant. Since hypocentral distance L_i is widely used in empirical attenuation functions of ground motions (e.g., Si and Midorikawa 1999; Boatwright 2007; Yabe et al. 2014), we simply assumed geometrical spreading $1/L_i$ of body waves, rather than inverse of exact ray-path length. Figure 1b shows the apparent attenuations for *P* and *S* waves estimated by least square fitting.

Figure 1c, d shows the measured *P*- and *S*-wave amplitudes and master attenuation curves as a function of the hypocentral distance for frequencies of 0.5–1 and 4–8 Hz. The color scale represents the magnitude of the *P*- and *S*-wave radiation pattern coefficients ($|F_P|$ and $|F_S|$; Aki and Richards 2002) estimated from MT solutions in the one-dimensional (1D) crustal velocity structure (Ukawa et al. 1984), which is used in the Hi-net routine hypocenter analysis. The *S*-wave radiation pattern coefficient $|F_S|$ was calculated by RMS of *SV*- and *SH*-wave radiation pattern coefficients. Wavelengths in Fig. 1c, d (λ_P and λ_S, respectively) were calculated by using the central frequencies of each band and seismic velocities in the crust. Observed amplitudes are scattered around master attenuation curves, reflecting the effects of non-isotropic source radiation and fluctuation of amplitude due to small-scale velocity inhomogeneity along propagation path (e.g., Hoshiba 2000; Yoshimoto et al. 2015).

The scatter due to non-isotropic source radiation is most evident in the *P*-wave amplitudes for the lowest frequency (0.5–1 Hz; left side of Fig. 1c). We confirmed that *P*-wave amplitudes with larger/smaller $|F_P|$ values tend to distribute above/below the master attenuation curve, respectively. As the frequency increased (4–8 Hz; right of Fig. 1c), this tendency become unclear, implying that *P*-wave amplitudes at higher frequencies do not show a clear four-lobe apparent radiation pattern. Although

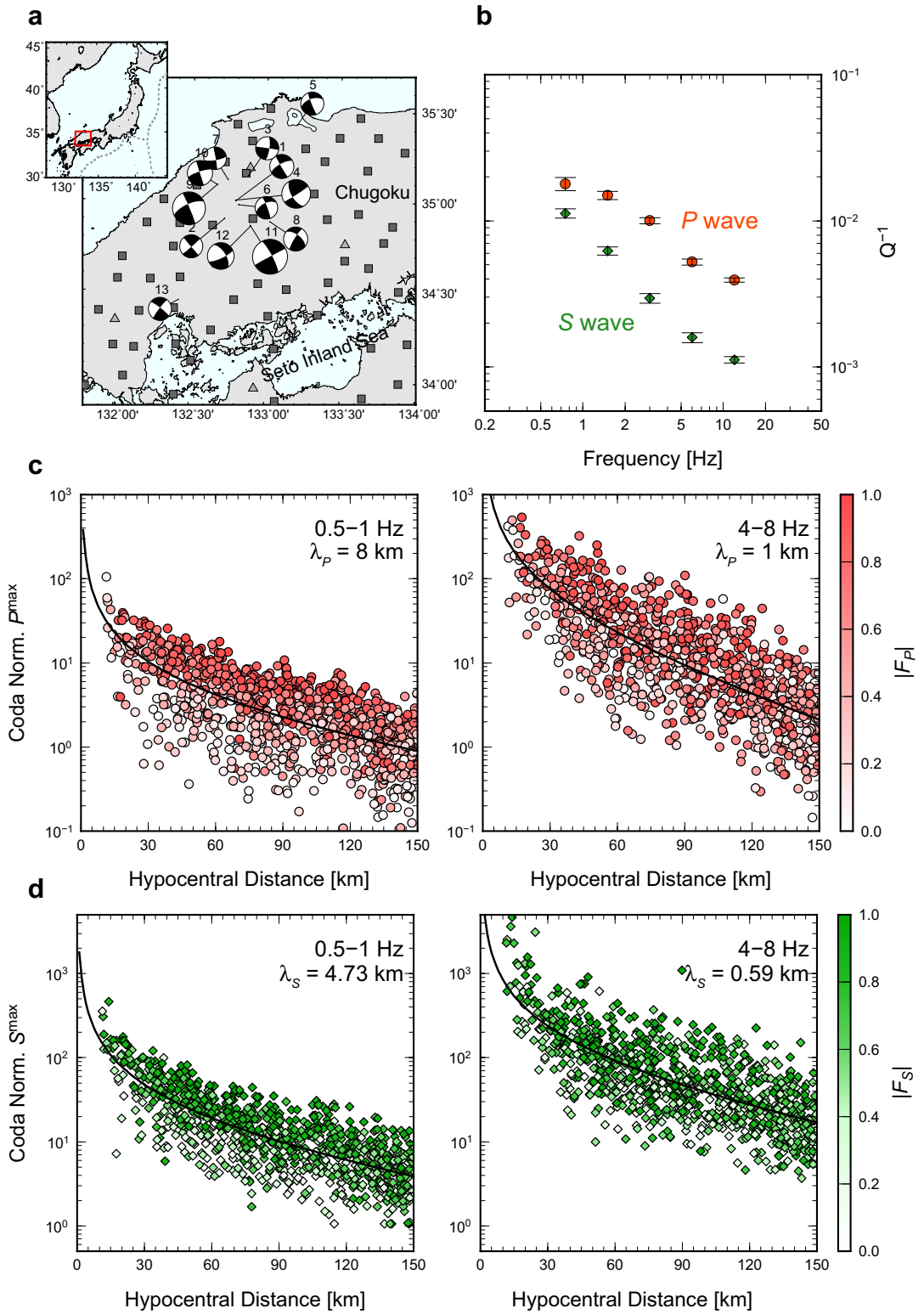

Fig. 1 Attenuation for maximum amplitudes of *P* and *S* waves. **a** Map of stations and epicenters, **b** estimated apparent attenuation for *P* and *S* waves as a function of frequency, and **c**, **d** amplitude attenuations for *P* and *S* waves, respectively. *Gray squares* and *triangles* in **a** denote the Hi-net and F-net stations, respectively. Focal mechanisms of each earthquake are referred from MT solutions of F-net. $|F_P|$ and $|F_S|$ are the magnitudes of respective *P*- and *S*-wave radiation pattern coefficients expected from MT solutions of the F-net in the 1D crustal structure (Ukawa et al. 1984; Aki and Richards 2002)

similar behaviors appeared in the *S*-wave amplitudes (Fig. 1d), the four-lobe patterns become unclear more rapidly compared to the *P*-wave ones (Fig. 1c).

We calculated the observed "amplitude fluctuation δA_j" by the following equation:

$$\delta A_j(L_i) = \frac{A_j(L_i) - A_{0j}(L_i)}{A_{0j}(L_i)} \left(j = P, S\right), \tag{2}$$

where $A_j(L_i)$ is the *P*- and *S*-wave amplitude at a hypocentral distance of L_i and $A_{0j}(L_i)$ is the prediction from the master attenuation curve (Eq. 1). Theoretical amplitude fluctuations were defined as $|F_j|$ fluctuations from the azimuthal average of $|F_j|$ at a hypocentral distance of L_i.

Figure 2 shows the comparison of azimuthal dependence of the observed and theoretical amplitude fluctuations (filled and open symbols, respectively) at frequencies of 0.5–1 and 4–8 Hz. Despite of the continuous four-lobe azimuthal variations of theoretical amplitude fluctuations, observed fluctuations are scattered around the theoretical ones. As wavelengths decrease, observed amplitude fluctuations are widely scattered and large amplitude fluctuations also appeared in the nodal directions. We confirmed that one of the key parameters for distortions of the observed *P*- and *S*-wave apparent radiation patterns is the wavelength of the seismic waves.

Frequency and distance dependences in the apparent radiation pattern

To quantify distortion of the apparent radiation pattern from double-couple point source predictions, we simply calculated the cross-correlation coefficient (CCC) between the observation and theoretical amplitude fluctuations using moving hypocentral distance windows (40–70, 50–80, 60–90, 70–100, 80–110, 90–120, and 100–130 km). Figure 3 shows the estimated CCCs as a function of the normalized hypocentral distance *kL*, where *k* is the wave number ($k = 2\pi/\lambda = 2\pi f/V$) and *L* is the average hypocentral distance of each distance range. Observed CCCs showed linear decay from 0.75 to 0.25 with increasing $\log(kL)$ from 1.64 to 2.85 and no significant differences in decay patterns between *P* and *S* waves. These results suggest that major causes of the frequency- and distance-dependent distortion of the apparent radiation pattern are seismic wave scattering and diffraction in the heterogeneous crust and that effects of crustal heterogeneity are not different for both *P* and S waves. Saturation of CCC decay was found at greater normalized hypocentral distances ($\log(kL) > 2.85$), showing almost dissipation of non-isotropic source radiation effect. Considering typical correlation length *a* of crustal heterogeneities (e.g., Takemura et al. 2009; Kobayashi et al. 2015), this feature appears in the strong scattering domain of *ka*–*kL* diagram (Fig. 13.11 of Aki and Richards 1980), in where conventional ray theory does not stand.

To characterize observed *kL* dependence of CCC, a linear fitting approach was applied by using the following equation:

$$\mathrm{CCC} = r\log(kL) + \mathrm{CCC}_0. \tag{3}$$

The values of *r* and CCC_0 were determined as -0.38 ± 0.023 and 1.35 ± 0.053, respectively, by a least squares estimation for the range of $\log(kL) < 2.85$. The observed CCC could be described by using resultant Eq. (3) (blue line in Fig. 3). We here introduce a set of values k_1L_1, k_2L_2, and k_3L_3 from $\log(k_iL_i) = 0.92$, 2.85, and 3.55 ($i = 1, 2, 3$), respectively, from Fig. 3, for the following discussions.

Apparent radiation pattern modeling and amplitude predictions

Pulido and Kubo (2004) proposed a simple linear frequency-dependent model of *S*-wave radiation pattern coefficients for strong ground motion prediction. On the basis of the observed linear decay of CCCs against $\log(kL)$, we revisited their approach and proposed a new model, which includes the frequency- and distance-dependent characteristics of the *P*- and *S*-wave apparent radiation pattern. Our frequency- and distance-dependent apparent radiation pattern coefficient R_j ($j = P, S$) at a station with a takeoff angle θ and azimuth ϕ is described by the following equation:

$$R_j(\theta,\phi,kL) = \begin{cases} F_j(\phi_S,\delta,\lambda,\theta,\phi), & \text{if } kL \le k_1L_1 \\ F_j(\phi_S,\delta,\lambda,\theta,\phi) - \frac{\log(kL)-\log(k_1L_1)}{\log(k_3L_3)-\log(k_1L_1)}\left(F_j^{\mathrm{ave}} - F_j(\phi_S,\delta,\lambda,\theta,\phi)\right), & \text{if } k_1L_1 \le kL \le k_2L_2 \\ F_j(\phi_S,\delta,\lambda,\theta,\phi) - \frac{\log(k_2L_2)-\log(k_1L_1)}{\log(k_3L_3)-\log(k_1L_1)}\left(F_j^{\mathrm{ave}} - F_j(\phi_S,\delta,\lambda,\theta,\phi)\right), & \text{if } k_2L_2 \le kL \end{cases}, \tag{4}$$

where F_j is the radiation pattern coefficient of a double-couple point source in the 1D crustal velocity structure (Ukawa et al. 1984). The focal mechanism is characterized by using angles of strike ϕ_S, dip δ, and rake λ. F_j^{ave} is the average radiation pattern coefficient for *P* and *S* waves of a double-couple point source (Boore and Boatwright 1984). Takeoff angle θ was also evaluated in the 1D structure model (an example shown in Fig. 4d). The modeled apparent radiation pattern coefficient introduced here is identical to the double-couple point source radiation pattern at small normalized hypocentral distances ($< k_1L_1$) and diminishes non-isotropy as increasing normalized hypocentral distance. Furthermore, our

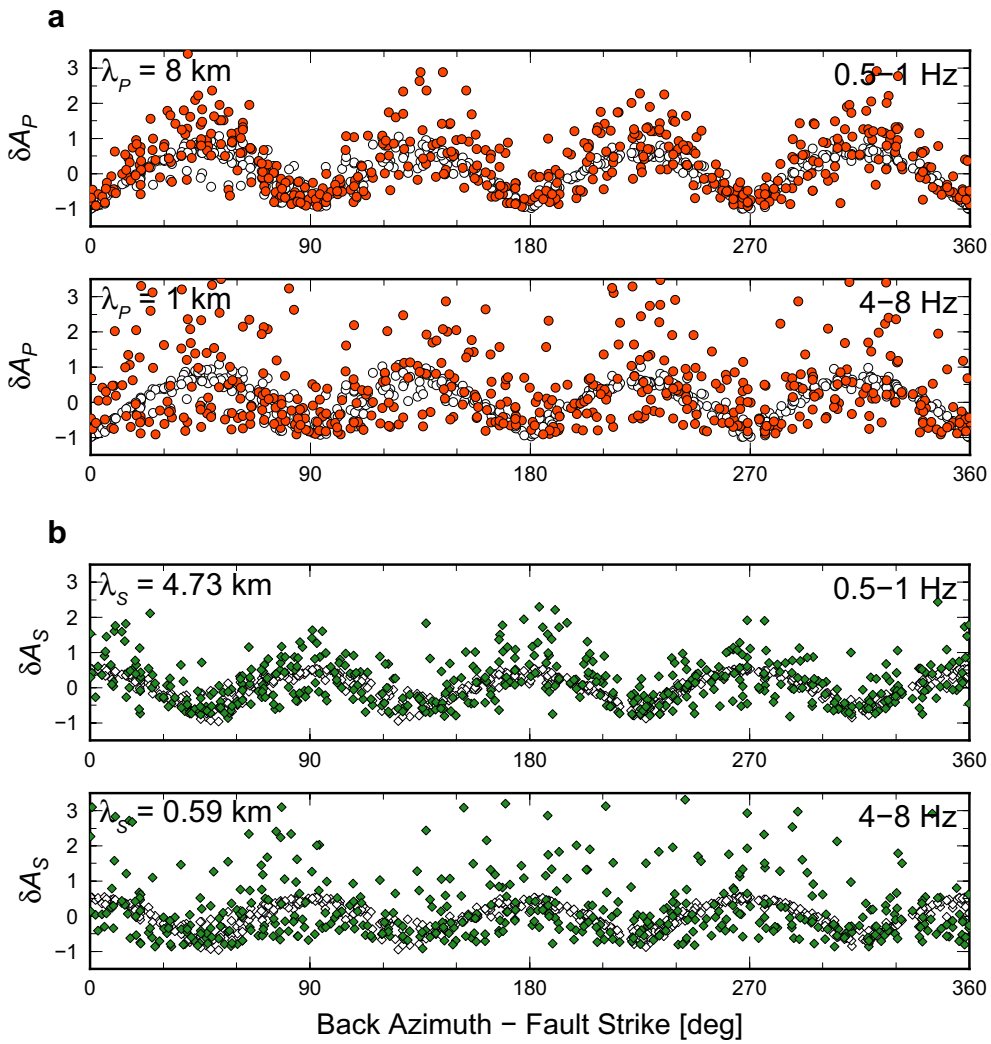

Fig. 2 Azimuthal dependence in the observed and theoretical fluctuations; **a** *P* and **b** *S* waves derived from data at hypocentral distances of 30–100 km during Events 1–13. *Filled* and *open symbols* represent observed and theoretical fluctuations, respectively

model includes not only *S*-wave radiation pattern but also *P*-wave one, which would be important for the earthquake early warning.

Figure 4a, b shows the spatial distributions of modeled apparent radiation pattern coefficients for frequencies of 0.5–1 and 4–8 Hz, respectively. We also show the spatial distribution of the radiation pattern coefficient for a double-couple point source in a homogeneous medium as a reference (Fig. 4c), where amplitude nodes ($R_j = 0.00$) clearly exist. The azimuthal difference of modeled apparent radiation pattern coefficients became unclear with increasing distances and wave numbers.

By using the estimated master attenuation curves and modeled apparent radiation pattern coefficients, we here propose a representation for the prediction of coda-normalized maximum amplitudes for both *P* and *S* waves $[A_j^{\max}(\theta, \phi, kL)]$ during local crustal earthquakes as follows:

$$A_j^{\max}(\theta,\phi,kL) = \frac{\delta R_j(\theta,\phi,kL)}{d_i} exp\left[-\frac{kL}{2Q_j(k)} + B\right]$$
$$\delta R_j(\theta,\phi,kL) = \frac{R_j(\theta,\phi,kL) - R_{0j}(kL)}{R_{0j}(kL)} \quad (5)$$

where $R_{0j}(kL)$ is the azimuthal average of the modeled apparent radiation pattern coefficient.

Figure 5 shows the comparisons between the observed and predicted spatial distributions of *P*- and *S*-wave amplitudes during Events 11 and 14 for low (0.5–1 Hz) and high (4–8 Hz) frequencies. The latter event was not

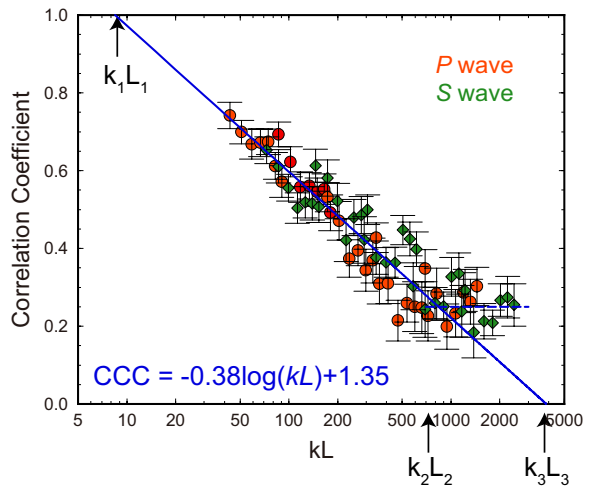

Fig. 3 Normalized distance (*kL*) dependence in CCCs between observed and theoretical fluctuations. Estimation error of CCC was evaluated by using the bootstrap method (Efron and Tibshirani 1986). Averaged CCC and estimation error were calculated for 100 sets of random resampling data

used in the analyzes of the apparent radiation patterns in the previous sections, and its source parameters are shown at the bottom of Additional file 1: Table S1. The effects of rupture directivity (e.g., Boatwright 2007; Pacor et al. 2016) and fluctuation of maximum amplitudes (e.g., Hoshiba 2000; Yoshimoto et al. 2015) were not taken into consideration within our method. Actually, for some earthquakes, directivity amplifications were found in the south–southeast direction from the source even for high frequencies (4–8 Hz). Recent observation study by Pacor et al. (2016) demonstrated that some earthquakes with Mw of 3.5–4 show directivity effects and that weakening of directivity starts at a frequency of approximately 10 Hz. Despite this, our predictions reproduced the observed spatial distributions of *P*- and *S*-wave amplitudes for both low- and high-frequency bands reasonably. Since seismograms with hypocentral distances less than 150 km were used in our analysis, practical applicability of our method is limited within same distance range. As the wave number ($k = 2\pi/\lambda = 2\pi f/V$) and distance ($L$) increased, both the observed and predicted maximum amplitude distributions became gradually distorted from the original four-lobe pattern of the double-couple point source.

Satoh (2014) employed frequency- and distance-dependent *S*-wave radiation pattern coefficient for the stochastic Green's function method based on empirical model of Satoh (2002a, b), which showed very weak distance dependency for frequencies of 2–5 Hz and an

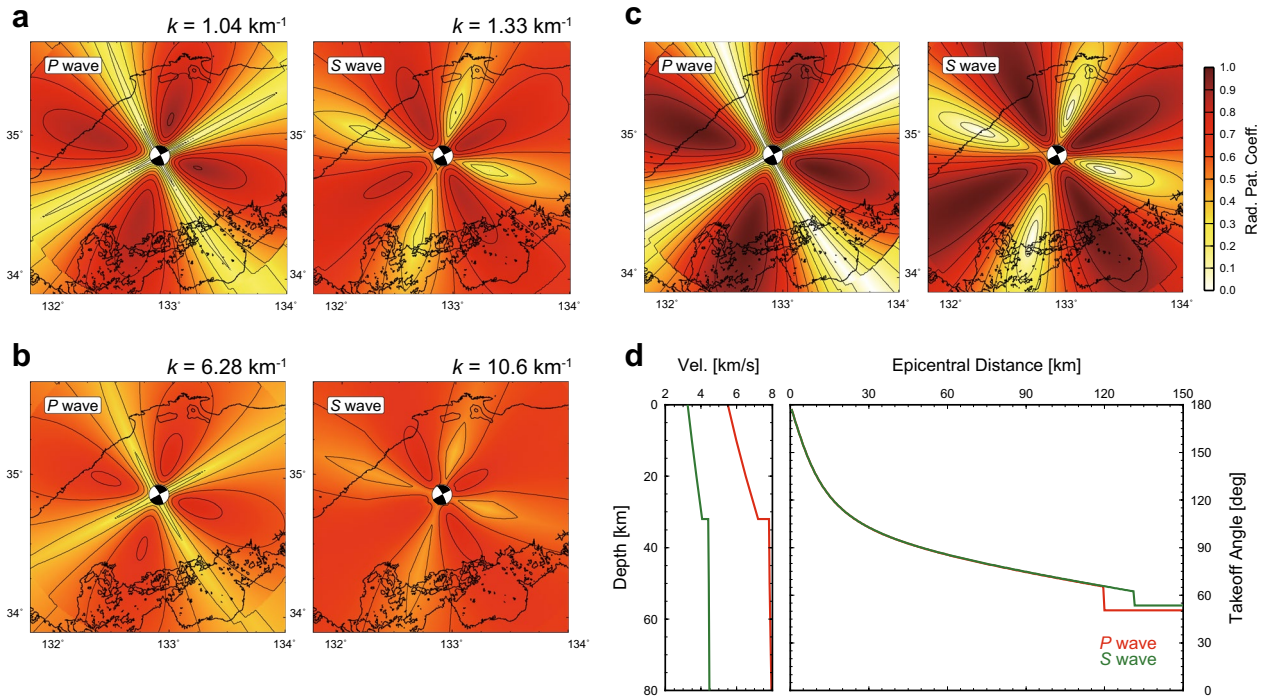

Fig. 4 Spatial distributions of modeled radiation pattern coefficients. Frequency ranges are **a** 0.5–1 and **b** 4–8 Hz, respectively. Theoretical radiation pattern coefficients in infinite homogeneous medium are also plotted in **c**. **d** Assumed one-dimensional velocity structure model (Ukawa et al. 1984) and calculated takeoff angles of Event 11 (depth of 11 km)

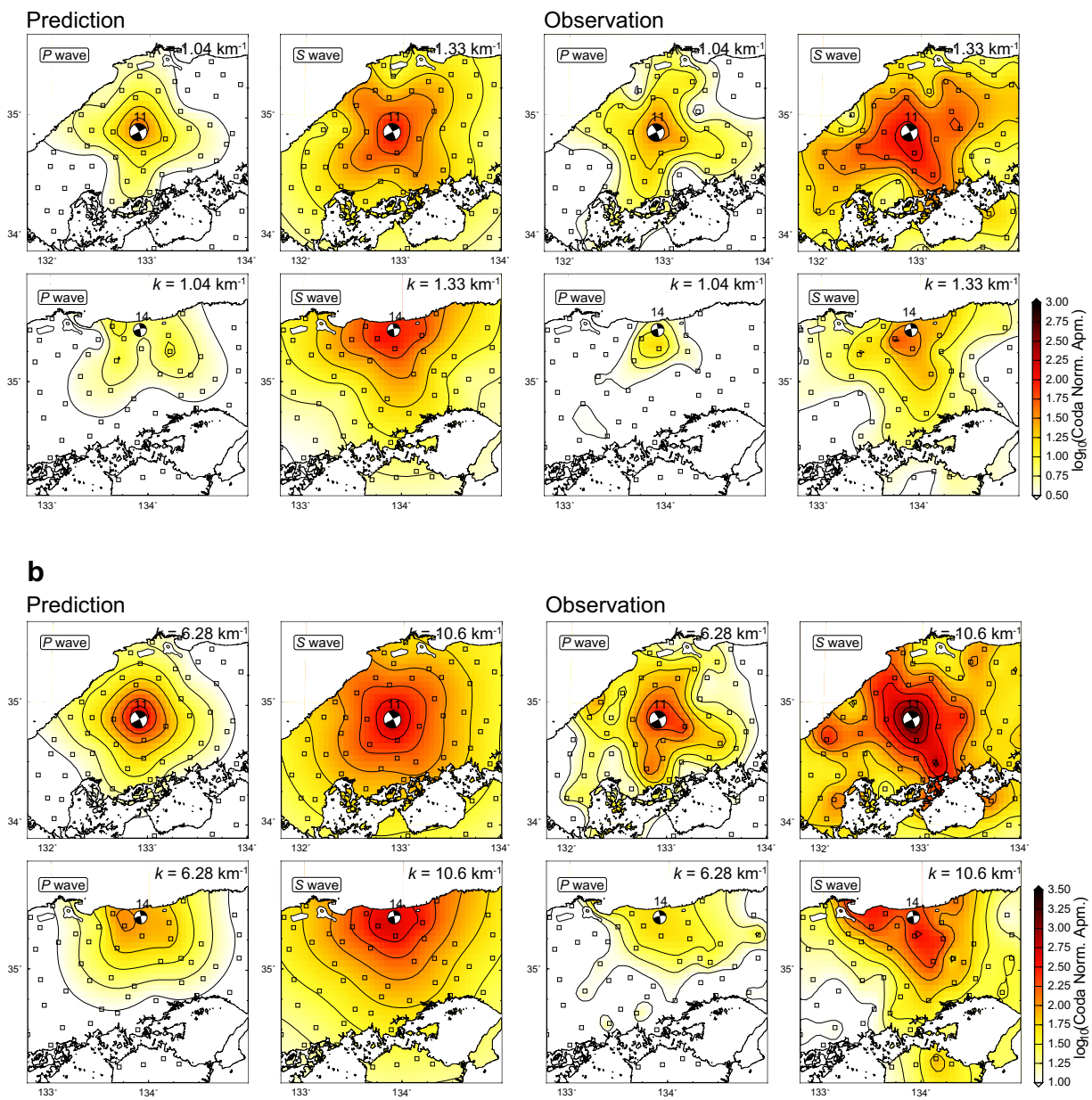

Fig. 5 Comparison between predicted and observed maximum amplitudes. Spatial distributions of coda-normalized *P*- and *S*-wave amplitudes for frequencies of **a** 0.5–1 and **b** 4–8 Hz during Events 11 and 14

isotropic radiation pattern for higher (>6 Hz) frequencies irrespective of distance. Satoh (2002b) constructed this model via observed energy partitioning of *S* waves in each horizontal component to reduce source and site amplification effects, rather than spatial distribution of maximum amplitude. Although our model does not include directivity effects, our model practically succeeds in reproducing observed spatial distribution of maximum amplitude of small-to-moderate local crustal earthquakes compared to Satoh (2002b)'s model (Additional file 1: Figure S2). This difference may be caused by difference in the method for model construction.

Conclusions

We investigated the frequency and distance dependences in the apparent radiation pattern for both *P* and *S* waves during local crustal earthquakes. We demonstrated how the four-lobe apparent radiation pattern, which is

expected from a double-couple point source, is gradually distorted with increasing frequency and distance. The observed distortions have common decay pattern for *P* and *S* waves and could be characterized by the normalized hypocentral distance *kL*. These results suggest that major causes of frequency- and distance-dependent distortion of the apparent radiation pattern are seismic wave scattering and diffraction in the heterogeneous crust.

The observed frequency and distance dependences in the apparent radiation patterns for both *P* and *S* waves could be simply modeled by using a linear function of log(*kL*). On the basis of this, we proposed a method for prediction of the spatial distributions of maximum *P*- and *S*-wave amplitudes. Our method, which incorporates frequency- and distance-dependent characteristics of the observed apparent radiation pattern, successfully reproduced the observed spatial distributions of *P*- and *S*-wave amplitudes during small-to-moderate local crustal earthquakes.

Our method could also provide better insights into source rupture process and practical correction for the effects of the apparent radiation pattern. In future study, this would enable us to estimate the radiated source energy precisely and to obtain better insights into high-frequency seismic sources, such as small earthquakes and non-volcanic/volcanic tremors and the other effects, especially rupture directivity and fluctuation of maximum amplitudes, will be taken into consideration within our method.

Additional file

Additional file 1: Figure S1 shows examples of observed waveforms and seismogram envelopes. **Figure S2** illustrates predicted maximum S-wave amplitudes based on radiation pattern coefficient of Satoh (2002b). The earthquakes used in our study are listed in **Table S1**.

Authors' contributions

ST developed basic idea of this work, proposed a new method for amplitude prediction, and drafted this manuscript. MK analyzed Hi-net/F-net waveform data and examined the characteristics of the apparent radiation pattern. KY made comments on seismic wave scattering and helped drafting. All authors read and approved the final manuscript.

Author details

[1] National Research Institute for Earth Science and Disaster Resilience, 3-1 Tennodai, Tsukuba 305-0006, Japan. [2] Department of Material System Science, Graduate School of Nanobioscience, Yokohama City University, 22-2 Seto, Kanazawa-ku, Yokohama 236-0027, Japan.

Acknowledgements

Hi-net and F-net waveform data and the MT solutions from the F-net are available via the Web site of the National Research Institute for Earth Science and Disaster Resilience, Japan. We used the unified hypocentral catalog provided by the Japan Meteorological Agency (JMA), which is available via the JMA server. The frequency response of the short-period Hi-net sensors with a natural frequency of 1 Hz was corrected to make a broadband record using the program of Maeda et al. (2011). Generic Mapping Tools (Wessel and Smith 1998) and Seismic Analysis Code (SAC) were used for making the figures and conducting the signal processing work, respectively. We also thank two anonymous reviewers and the editor Prof. H. Takenaka for careful reading and constructive comments that improved the manuscript.

Competing interests

The authors declare that they have no competing interests.

Received: 29 April 2016 Accepted: 8 October 2016
Published online: 21 October 2016

References

Aki K, Richards P (1980) Quantitative seismology. University Science Books, Freeman, San Francisco

Aki K, Richards P (2002) Quantitative seismology, 2nd edn. University Science Books, Freeman, San Francisco

Boatwright J (2007) The persistence of directivity in small earthquakes. Bull Seismol Soc Am 97:1850–1861. doi:10.1785/0120050228

Boore DM, Boatwright J (1984) Average body-wave radiation coefficients. Bull Seismol Soc Am 74:1615–1621

Cannata A, Frazia DG, Aliotta M, Cassisi C, Montalto P, Patane D (2013) Monitoring seismo-volcanic and infrasonic signals at volcanoes: Mt. Etna case study. Pure appl Geophys 170:1751–1771. doi:10.1007/s00024-012-0634-x

Efron B, Tibshirani R (1986) Bootstrap methods for standard errors, confidence intervals, and other measures of statistical accuracy. Stat Sci 1(1):54–77

Fukuyama E, Ishida M, Dreger DS, Kawai H (1998) Automated seismic moment tensor determination by using on-line broadband seismic waveforms. Zisin 51:149–156 **(in Japanese with English abstract)**

Hoshiba M (2000) Large fluctuation of wave amplitude produced by small fluctuation of velocity structure. Phys Earth Planet Int 120:201–217. doi:10.1016/S0031-920(99)00165-X

Kobayashi M, Takemura S, Yoshimoto K (2015) Frequency and distance changes in the apparent *P*-wave radiation pattern: effects of seismic wave scattering in the crust inferred from dense seismic observations and numerical simulations. Geophys J Int 202:1895–1907. doi:10.1093/gji/ggv263

Kumagai H, Nakano M, Maeda T, Yepes H, Palacios P, Ruiz M, Arrais S, Vaca M, Molina I, Yamashita T (2010) Broadband seismic monitoring of active volcanoes using deterministic and stochastic approaches. J Geophys Res 115:B08303. doi:10.1029/2009JB006889

Liu H, Helmberger DV (1985) The 23:19 aftershock of the 15 October 1979 Imperial Valley earthquake: more evidence for an asperity. Bull Seismol Soc Am 75:689–708

Maeda T, Obara K (2009) Spatiotemporal distribution of seismic energy radiation from low-frequency tremor in western Shikoku, Japan. J Geophys Res 114, B00A09, doi:10.1029/2008JB006043

Maeda T, Obara K, Furumura T, Saito T (2011) Interference of long-period seismic wavefield observed by the dense Hi-net array in Japan. J Geophys Res 116:B10303. doi:10.1029/2011JB008464

Nakahara H (2013) Envelope inversion analysis for high-frequency seismic energy radiation from the 2011 M_W 9.0 Off the Pacific Coast of Tohoku earthquake. Bull Seismol Soc Am 103:1348–1359. doi:10.1785/0120120155

Ogiso M, Yomogida K (2015) Estimation of locations and migration of debris flows on Izu-Oshima Island, Japan, on 16 October 2013 by distribution of high frequency seismic amplitude. J Volc Geotherm Res 298:15–26. doi:10.1016/j.jvolgeores.2015.03.015

Okada Y, Kasahara K, Hori S, Obara K, Sekiguchi S, Fujiwara H, Yamamoto A (2004) Recent progress of seismic observation networks in Japan—Hi-net, F-net, K-NET and KiK-net. Earth Planets Space, 56, xv–xxviii, doi:10.1186/BF03353076

Okamoto K, Tsuno S (2015) Investigation on relationship between epicentral distance and growth curve of initial *P*-wave propagating in local heterogeneous media for earthquake early warning system. Earth Planets Space 67:167. doi:10.1186/s40623-015-0339-3

Pacor F, Gallovič F, Puglia R, Luzi L, D'Amico M (2016) Diminishing high-frequency directivity due to a source effect: empirical evidence from small

earthquakes in the Abruzzo region Italy. Geophys Res Lett 43:5000–5008. doi:10.1002/2016GL068546

Pitarka A, Somerville P, Fukushima Y, Uetake T, Irikura K (2000) Simulation of near-fault strong-ground motion using hybrid Green's functions. Bull Seismol Soc Am 90:566–586. doi:10.1785/0119990108

Pulido N, Kubo T (2004) Near-fault strong motion complexity of the 2000 Tottori earthquake (Japan) from a broadband source asperity model. Tectonophysics 390:177–192. doi:10.1016/j.tecto.2004.03.032

Sato H, Fehler M, Maeda T (2012) Seismic wave propagation and scattering in the heterogeneous earth structure, 2nd edn. Springer, Berlin

Satoh T (2002a) Empirical frequency-dependent radiation pattern of the 1998 Miyagiken-Nanbu earthquake in Japan. Bull Seismol Soc Am 92:1032–1039. doi:10.1785/0120010153

Satoh T (2002b) Radiation pattern and f_{max} of the Tottori-ken Seibu earthquake and the aftershocks inferred from KiK-net strong motion records. J. Struct Constr Eng AIJ 556:25–34 **(in Japanese with English abstract)**

Satoh T (2014) Generation method of stochastic Green's function considering into surface waves and scattering waves using records of moderate-size interplate earthquakes along the Sagami Trough. J Struct Constr Eng AIJ 705:1589–1599 **(in Japanese with English abstract)**

Sawazaki K, Sato H, Nishimura T (2011) Envelope synthesis of short-period seismograms in 3-D random media for a point shear dislocation source based on the forward earthquakes in southwestern Japan. J Geophys Res 116:B08305. doi:10.1029/2010JB008182

Si H, Midorikawa S (1999) New attenuation relationships for peak ground acceleration and velocity considering effects of fault type and site condition. J Struct Constr Eng AIJ 523:63–70 **(in Japanese with English abstract)**

Takemoto T, Furumura T, Saito T, Maeda T, Noguchi S (2012) Spatial- and frequency-dependent properties of site amplification factors in Japan derived by coda normalization method. Bull Seismol Soc Am 102:1462–1476. doi:10.1785/0120110188

Takemura S, Furumura T, Saito T (2009) Distortion of the apparent S-wave radiation pattern in the high-frequency wavefield: Tottori-ken Seibu, Japan, earthquake of 2000. Geophys J Int 178:950–961. doi:10.1111/j.1365-246X.2009.04210.x

Takemura S, Furumura T, Maeda T (2015) Scattering of high-frequency seismic waves caused by irregular surface topography and small-scale velocity inhomogeneity. Geophys J Int 201:459–474. doi:10.1093/gji/ggv038

Takenaka H, Mamada Y, Futamure H (2003) Near-source effect on radiation pattern of high-frequency S waves: strong SH–SV mixing observed from aftershocks of the 1997 Northwestern Kagoshima, Japan, earthquakes. Phys Earth Planet Int 137:31–43. doi:10.1016/S0031-9201(03)00006-2

Ukawa M, Ishida M, Matsumura S, Kasahara K (1984) Hypocenter determination method of the Kanto-Tokai observational network for microearthquakes. Res Notes Natl Res Cent Disaster Prev 53:1–88 **(in Japanese with English abstract)**

Wessel P, Smith WHF (1998) New, improved version of generic mapping tools released, *EOS*. Trans Am Geophys Union 79:579. doi:10.1029/98EO00426

Yabe S, Ide S (2014) Spatial distribution of seismic energy rate of tectonic tremors in subduction zones. J Geophys Res 119:8171–8185. doi:10.1002/2014JB011383

Yabe S, Baltay A, Ide S, Beroza G (2014) Seismic-wave attenuation determined from tectonic tremor in multiple subduction zones. Bull Seismol Soc Am. doi:10.1785/0120140032

Yoshimoto K, Sato H, Ohtake M (1993) Frequency-dependent attenuation of P and S waves in the Kanto area, Japan, based on the coda-normalization method. Geophys J Int 114:165–174. doi:10.1111/j.1365-246X.1993.tb01476.x

Yoshimoto K, Takemura S, Kobayashi M (2015) Application of scattering theory to *P*-wave amplitude fluctuations in the crust. Earth Planets Space 67:199. doi:10.1186/s40623-015-0366-0